Science program of the AMBER consortium

Fabien Malbet, Thomas M. Driebe, Renaud Foy, Didier Fraix-Burnet, Philippe Mathias, Alessandro Marconi, Jean-Louis Monin, Romain G. Petrov, Philippe Stee, Leonardo Testi, et al.

Science program of the AMBER consortium

Fabien Malbet[a], Thomas Driebe[b], Renaud Foy[c], Didier Fraix-Burnet[a], Philippe Mathias[d], Alessandro Marconi[e], Jean-Louis Monin[a], Romain Petrov[f], Philippe Stee[d], Leonardo Testi[e] and Gerd Weigelt[b]

[a]LAOG, Laboratoire d'Astrophysique de Grenoble, BP 53, F-38041 Grenoble, France;
[b]MPIfR, Max-Planck für Radioastronomie, Bonn, Germany;
[c]CRAL, Centre de Recherche en Astrophysique de Lyon, Lyon, France;
[d]OCA, Observatoire de la Côte d'Azur, Laboratoire Gemini, Nice, France ;
[e]OAA, Osservatorio Astrofisico di Arcetri, Firenze, Italy;
[f]LUAN, Laboratoire Universitaire d'Astrophysique de Nice, Nice, France;

ABSTRACT

AMBER had first light in March 2004. The guaranteed time observations of the AMBER consortium (LAOG, MPIfR, OAA, OCA, UNSA) consists of 87 proposals ranging from cosmology, extragalactic studies, star formation, planetary system, late stages of stellar evolution to physical properties of stars. Some examples, AGN, evolved stars and hot stars are discussed in this paper.

Keywords: Astrophysics, Optical interferometry, High angular resolution

1. INTRODUCTION

AMBER is one of the first-generation instruments of the *Very Large Telescope Interferometer (VLTI)* that has been described by Petrov et al.[1, 2] The science program which has been prepared has already partly been described by Malbet et al.[3] in a previous SPIE paper. Here we complement this information with an overview of AMBER capability, some details on how the AMBER science program has been defined (Sect. 2) and specific examples of this program on AGN (Sect. 3), evolved stars (Sect. 4) and hot stars (Sect. 5).

AMBER is an interferometric beam combiner for the VLTI working in the near-infrared J, H, K bands. It is able to handle simultaneously 3 beams coming from 3 identical telescopes. AMBER interferograms are spectrally dispersed with a resolution of about 35, 1200 and 10000. Therefore AMBER can measure vibilities and a closure phase in a few hundred different spectral channels.

The main characteristics of AMBER on the VLTI are:

- **Angular resolution:** Angular resolution is set by the maximum available baseline, which is about 200 meters for the ATs and about 130 meters for the UTs. Accordingly, the K-band resolution limit will be about 2 milliarcseconds (mas) for the ATs, and about 3 mas for the UTs.
- **Number of baselines:** A second important factor that characterizes the performance of an interferometer is the number of available baselines. In the case of VLTI, the large number of stations for the ATs and the availability of four UTs, provides a very rich scenario of possible baselines. Altogether, 254 independent baselines are possible.
- **Spectral configuration:** AMBER has 3 spectral resolution (35, 1500 and 10000) and 3 spectral bands J, H, and K. In fact, in the low resolution mode the observer has access to the 3 bands simultaneously. The 7 spectral configurations are: JHK-LR for the low resolution, J-MR, H-MR, and K-MR for the medium resolution, and J-HR, H-HR, and K-HR for the high resolution.

Send correspondence to F. Malbet
E-mail: fabien.malbet@obs.ujf-grenoble.fr

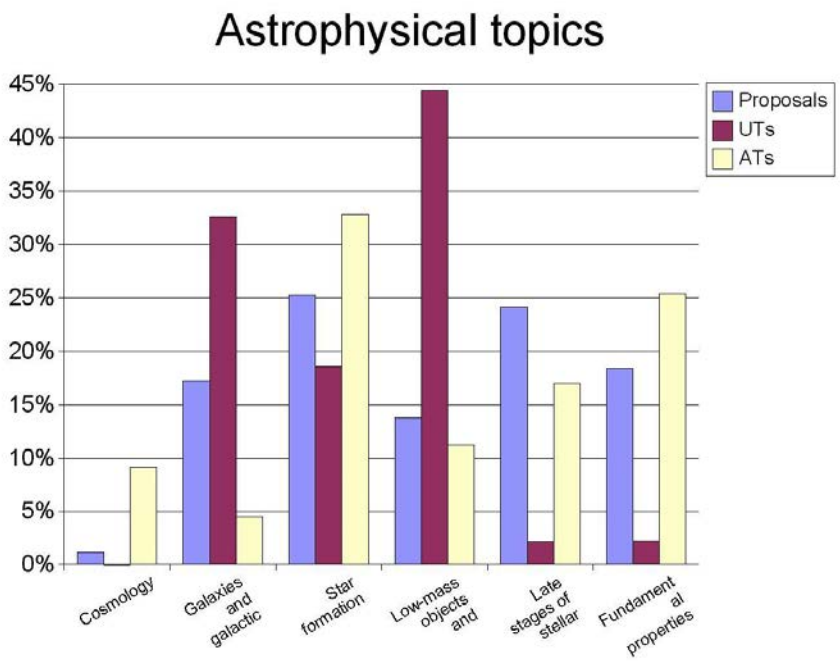

Figure 1. Distribution of astrophysical topics in phase B in percentage of number of proposals (left light gray bar), of UT time (middle dark gray bar) and of AT time (right white bar). *Note: t he AT time is the product of the number of telescopes used by the requested time for harmonization between the proposals. This convention is not no longer used in the following sections and figures unless explicitly quoted.*

- **Instrument modes:** depending on the type of science, one can choose to observe with AMBER in classical way or in wavelength differential mode. The differential mode involves slight differences in the observing procedures but allows the observers to obtain larger precision on the differential phase. The expected visibility accuracy is typically 1% for the high sensitivity mode, 0.1% for the high precision mode, and 0.01% for the phase in the high precision mode in the differential configuration.
- **Flux sensitivity:** concerning the limits in sensitivity, these depend on a large number of factors: exposure time (high sensitivity : 50ms, high precision : 10ms, and long exposures in the case of fringe tracking), the type of telescopes, the spectral resolution, the seeing, etc. In the case of off-axis reference tracking using the PRIMA dual-feed facility, the ability to observe the source depends on the possibility to find a reference source whose magnitude fulfills the limit.
- **Field of view:** AMBER is a single-mode instrument, therefore the field of view is limited to the Airy disk of each individual aperture, i.e. 250 mas for the ATs in K and 60 mas for the UTs in K.

2. BUILDING THE SCIENCE PROGRAM OF THE AMBER CONSORTIUM

The AMBER consortium had to prepare the first phase of AMBER observations. The consortium has access to 3 types of time on the VLTI:

- Guaranteed time (GT)
- Open time (OT)
- Science Demonstration Time (SDT)

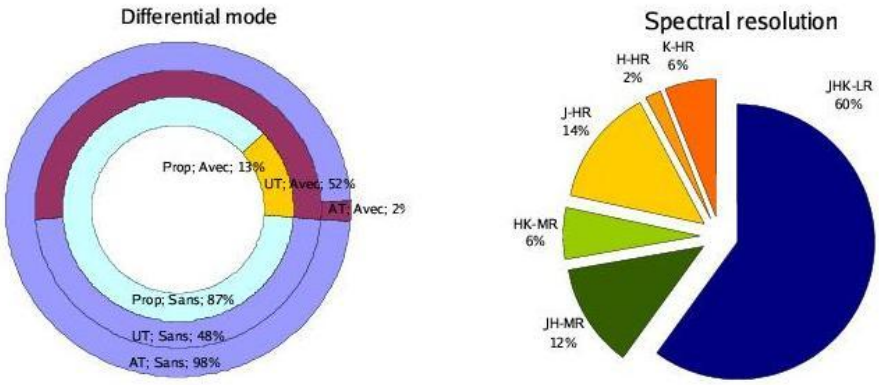

Figure 2. AMBER configurations requested during phase B call.

The science group of AMBER (SGR) is in charge of coordinating the proposals which come from the AMBER consortium under the responsability of the PI (R. Petrov) and the co-PIs (F. Lisi, F. Malbet, D. Mourard, and G. Weigelt). The SGR has therefore issued a call for proposals within the AMBER consortium with the aim of coordinating the different proposing teams and helping them to be ready on time. This call for proposals was divided in two phases in order to allow iterations:

- Phase A (July-December 2001): proposals with general ideas
- Phase B (July 2002-December 2002): detailed and coordinated proposals

For the phase A review, we received 102 submitted proposals . This high number of proposals shows the high interest of the astronomers within the AMBER consortium. 85% of the proposals had enough details to be reviewed.

For Phase B, we received a total of 87 proposals. Since some proposals requested 2 telescopes and other 3 ones, we took into account the total number of hours times the number of telescopes to present an homogenized table and not the number of hours of interferometer. We can derive some statistics:

- Requested telescope time:
  - Total requested UT time: 1255 hours of UT telescopes
  - Total requested AT time: 2842 hours of VISA array
- Telescope conFIguration:
  - 14 (16%) proposals requested 2 telescope conFIguration
  - 62 (71%) proposals requested 3 telescope conFIguration
  - 11 (13%) proposals requested a mix of 2 or 3 telescope configurations
- Differential calibration:
  - 11 versus 76 proposals required special dierential calibration tool
  - 692 versus 632.5 UT hours, ie 52% of UT time
  - 174 versus 8371.5 AT hours, ie 2% of AT time

  NB: The large amount of UT time comes from the exoplanet proposals (44-48).
- Spectral resolution (in hours of AMBER):

- 60% of low spectral resolution JHK-LR (2153.5 h)
- 18% of medium spectral resolution spread over:
  - 12% of JH-MR (443 h)
  - 6% of HK-MR (219.5 h)
- 22% of medium spectral resolution spread over:
  - 14% of J-HR (498 h)
  - 2% of H-HR (59 h)
  - 6% of K-HR (217.5 h)

The distribution of telescope time between the various astrophysical topics is displayed respectively in Fig. 1. From this phase B review, it was the possible to make build a science program which does not cover all potential topics, but the ones that are tackle by the teams of different AMBER institutes.

The total amount of requested time corresponds to the guaranteed time allocated by ESO to the AMBER consortium and written in the Memorandum of Understanding (MoU) signed between AMBER and ESO.

The number of GT UT nights is well defined and is 60 nights of individual telescopes. Since AMBER can be used either with 2 or 3 telescopes, we decided to count the UT time in hours of individual telescope and therefore with an average of 10h per night, it corresponds to a total of 600 h of UT.

Concerning the ATs, the ESO/AMBER MoU states that the AMBER consortium is rewarded a number of VISA (AT array) nights in proportion of its cost, minus the UT nights contribution. AMBER has a total GT corresponding to 4.62% of VISA time during 8 years, corresponding to a total number of 1350h of VISA (with an average of 10h per night). This does not depend on the number of telescopes, and therefore we decided to count the AT time in hours of interferometer time with an average of 10h per night, i.e. a total of 1350h of AT array.

The actual GTO program is now public and available on the AMBER web site at:

`http://www-laog.obs.ujf-grenoble.fr/heberges/amber`

under the menu *Amber Documents*.

3. ACTIVE GALACTIC NUCLEI

3.1. Dust environment of AGN

The nearest active galactic nuclei (AGN) are very important candidates for testing the predictions of unification schemes[4] of AGN. The main ingredient of these models is a geometrically and optically thick torus surrounding the central continuum source. This torus is able to obscure the central source if the angle between its polar axis and the observer's viewing direction is large enough. Such a torus would collimate radiation from the central source and lead to the ionization cone, which is visible, for example, in the Hubble Space Telescope [O III] image of NGC 1068. Theoretical studies of AGN tori were reported by many authors[5–7] (and references therein). One of the nearest and brightest Seyfert galaxies is NGC 1068 (distance of 14.4 Mpc, corresponding to a linear scale of $72\,\mathrm{pc\,arcsec^{-1}}$). During the last few years speckle interferometric observations, adaptive optics (AO), and long-baseline interferometry of the dust environment of NGC 1068 were reported.

In the following section we discuss a few of these NGC 1068 results in order to show that infrared interferometry is able to resolve the dust near the walls of a low-density outflow cavity or in the innermost region of a parsec-scale dusty torus. In particular, we discuss the speckle interferometric observations of the central NIR core of NGC 1068 which has a size of $\sim 30 \pm 8$ mas or ~ 2 pc[8–10] and the first K-band long-baseline interferometry.[11]

Near-infrared Adaptive Optics (AO) observations[12] of NGC 1068 have resolved an elongated north-eastern and east-western structure and have determined an upper limit of the K-band core diameter of ~ 9 pc. Bispectrum speckle interferometry observations[11] with the SAO 6 m telescope allowed the reconstruction of the first diffraction-limited K-band image with 76 mas resolution of the central 30 ± 8 mas (~ 2 pc) core of NGC 1068. The

reconstructed image is elongated and has a north-western tail at position angle (P.A.) of approximately –20°. L- and M-band images[13] obtained with the VLT and the NACO AO instrument show several new structures in the region of the radio jet, for example, a northern spiral arm-like structure and a southern tongue. VLBA observations of NGC 1068 at 8.4 GHz[14] with an angular resolution of $\sim 1 \times 2$ mas resolved the radio source S1, which is believed to be located at the position of the AGN. This source S1 has a size of $\sim 10 \times 30$ mas, and its long axis (P.A. $\sim 106°$) is approximately perpendicular to the inner radio jet. Astrometric studies have shown that the position of the 2.2 μm peak approximately coincides with the position of the MIR peak, as well as with the center of the HST polarization map and with the radio component S1 (see references in Ref. 7). These observations suggest that the position of the IR peak and the radio component S1 is the location of the central engine of the AGN and that the NIR and MIR core is emission from hot dust in the vicinity of the central engine.

H- and K'-band bispectrum speckle interferometry studies[10] of the nuclear region of NGC 1068 with the SAO 6 m telescope allowed the reconstruction of a diffraction-limited K'-band image with 74 mas resolution and the first H-band image with 57 mas resolution. The resolved structure consists of a compact core and an extended northern and south-eastern component. The compact core has a north-western, tail-shaped extension. The K'-band FWHM diameter of this compact core is 18×39 mas or 1.3×2.8 pc (the diameter errors are ± 4 mas), and the P.A. of the north-western extension is $-16 \pm 4°$. This P.A. is very similar to that of the western wall (P.A. $\sim -15°$) of the bright region of the ionization cone. This suggests that the H- and K'-band emission from the compact core is both thermal emission and scattered light from dust near the western wall of a low-density, conical cavity or from the innermost region of a parsec-scale dusty torus that is heated by the central source (the dust sublimation radius of NGC 1068 is approximately 0.1 – 1 pc). The northern extended 400 mas structure lies near the western wall of the ionization cone and coincides with the inner radio jet.

Finally, first long-baseline interferometry in the near-infrared K band[11] (VINCI beam combiner) and in the mid-infrared[15] (MIDI beam combiner) were carried out with two 8.2 m Unit Telescopes of ESO's VLT Interferometer. The VINCI K-band observations[11] show that the squared visibility amplitude of NGC 1068 is approximately 16 % at a projected baseline of 45.8 m. This visibility corresponds to a substructure of ≤ 5 mas or ≤ 0.4 pc. All these observations clearly show that NIR long-baseline interferometry with the VLTI and its phase closure instrument AMBER will allow us to study the environment of the central engine of the nearest AGN with unprecedented resolution.

3.2. The Broad Line Region of AGN

The BLR (Broad Line Region) is the region where the broad (FWHM> 1000 km/s) permitted lines observed in the spectra of type 1 AGNs originate (e.g.[16]). Given the small distance from the central super massive black hole (SMBH) the width of the broad lines is likely to originate from the gravitational motion of gas clouds around the SMBH. So far, the size of the BLR could not be directly measured and the only available information is provided by the so-called reverberation mapping technique (e.g.[17]). The BLR size is estimated as $c\Delta\tau$ where $\Delta\tau$ is the time lag between the continuum and line variation. Clearly this represents an average size weighted over the BLR geometry and physical conditions. In principle the BLR geometry and kinematics can be derived from the detailed behavior of the light curves, but the inversion is not unique mainly because of the correspondence between the 1-dimensional nature of light curves and the 3-dimensional nature of the BLR. Also the non optimal time sampling of the observations strongly reduces the constraints which can be derived. Suggested spatial distribution of the BLR clouds are spherical, disk-like or conical. Dynamically, the BLR might be dominated by gravitational motions (either a virialized system with chaotic motions or a disk in keplerian rotation), or might be part of a radiation pressure driven outflow, or of an inflow. Obtaining a direct measure of the BLR size and constraining its morphology and kinematics is fundamental in order to understand its origins and relationship with AGN activity, and to measure the mass of the SMBH and verify reverberation mapping techniques. BLR sizes determined with the reverberation mapping have been found to correlate with the quasar luminosity. A recent estimate by Kaspi et al.[18] gives:

$$R_{BLR} \sim 33 \left(\frac{\lambda L_\lambda (5100(5100\text{Å}))}{10^{44}\, erg\, s^{-1}} \right)^{0.7} \text{light days} \quad (1)$$

where L_λ is the rest-frame monochromatic luminosity at 5100 Å. Assuming a standard cosmology ($H_0 = 70$ km/s/Mpc, $\Omega_M = 0.3$ and $\Omega_\Lambda = 0.7$), R_{BLR} can be translated into an apparent size in the plane of the sky

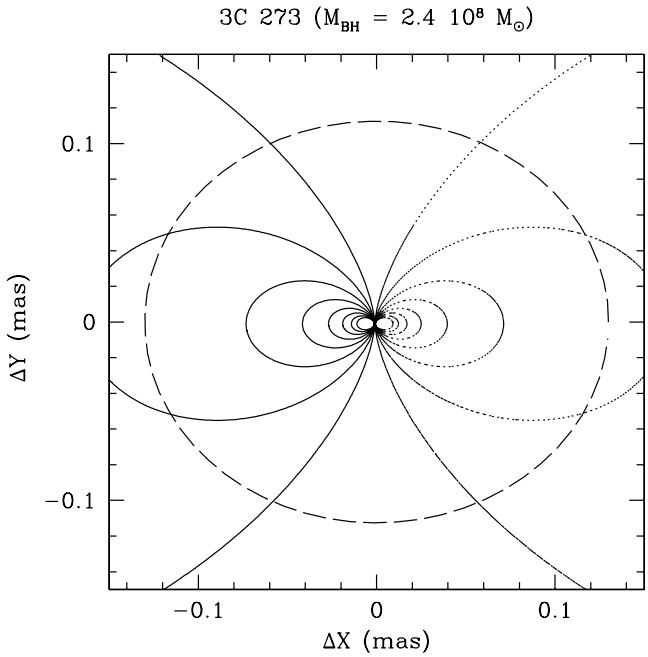

Figure 3. Isovelocity contours for the BLR of 3C273. 'Red' velocities are represented with a solid line, 'blue' velocities with a dotted line. Contours go from 400 to 3200 km/s with steps of 400 km/s. The dashed line is the BLR radius measured with reverberation mapping. The assumed disk inclination with respect to the line of sight is 30 deg.

obtaining for instance $R_{BLR} = 0.03$ mas for a $L = 10^{12}$ $L_\odot$ quasar at $z = 0.1$ (we have assumed $\lambda L_\lambda(5100\text{Å}) = L/15$). For $L = 10^{13}$ $L_\odot$ and $z = 0.5$, $R_{BLR} = 0.04$ mas. These numbers imply that BLRs are not resolvable with the VLTI. However, when a source is not resolved by an interferometer, the differential phase measures the displacement of the photocenter with wavelength along the baseline direction. This is valid even when this displacement is much smaller than the standard resolution limit of the interferometer. The position of the photocenter with wavelength is a powerful constraint for the geometry and kinematics of the BLR and can be obtained by taking advantage of the AMBER spectral resolution.

For example, one can consider the case of the famous quasar 3C273. Its BLR radius measured with reverberation mapping by,[18] $R_{BLR} = 387 \pm 55$ lt-days corresponds to 0.13 mas (at the distance of 3C 273, 1 mas corresponds to 2.6 pc) and the inferred BH mass is $\sim 2.4 \times 10^8$ $M_\odot$. Figure 3 shows the expected isovelocity contours with steps of 400 km/s assuming that the BLR is in a Keplerian disk and that it is inclined of 30 deg with respect to the line of sight. Using AMBER with Medium spectral resolution ($\mathcal{R} = 750$), one can measure the differential phase of the broad Paα in the K band and obtain information in 400 km/s velocity bins. At 2.2μm, with a projected baseline of 80 m, a photocenter displacement of 0.13 mas will result in a phase shift on the line of $\phi \sim 0.15$ rad. Since in each spectral channel we expect ~ 300 Paα photons/sec, the expected accuracy which can be reached in 1 h of observation is $\sigma_\phi \sim 0.002$ rad ($\sim 2\,\mu$arcsec in K with a 80 m baseline), thus allowing to measure the photocenter displacement. Since a given measure with two telescopes yields mainly one component of the photocenter displacement, in order to obtain a full map of the photocenter displacement one should measure the differential phase using observations from two perpendicular baselines.

The differential phase in each velocity bin will provide the position of the photocenter of the part of the disk which is delimited by two contiguous contours in figure 3. In this case, the photocenters will be aligned along the line of nodes of the disk and, combining positional and velocity information, one can directly measure the mass of the central BH. Conversely, if the BLR is composed by a spherically symmetric and isotropic ensemble of clouds the photocenters will all coincide with the position of the continuum photocenter and no differential phase will be measured. Other locations of the photocenters will result in more complicated geometries but, in any case, the amplitude of the photocenter displacement is directly related to the angular size of the BLR. If we

are able to establish a relationship between the differential interferometry angular radius and the reverberation mapping linear radius, we can get a direct measurement of the AGN distance. Since, in the best case, this kind of measurement can be made on a magnitude $V \sim 20$ quasar when there is a nearby reference star, this could eventually lead to a new and independent technique to measure cosmological distances.

4. EVOLVED STARS

4.1. Mira stars

Several features in the spectrum of Long Period Variable stars are interpreted since many decades as the signature of shock waves propagating through an extended atmosphere. Due to the complexity of physical mechanisms involved in these objects, model atmosphere are still in the infancy. A major step in this field will be to build semi-empirical models, with in particular information about the spatial structure and the propagation velocity of the shock wave(s) being provided from high angular resolution observations.

The VLTI high angular resolution together with its spectral resolution will provide these models with unique constraints. In particular the measure of the location of the shock wave(s) as a function of time is a critical input for dynamical model atmospheres. In the case of close targets, possible inhomogeneities perpendicular to the line of sight could be detected as well, which would provide us with some insight about the still unknown shock wave mechanism. AMBER and the VLTI are the only devices able to measure the extension and the geometry of those regions quite close to the innermost photosphere layers.

4.2. Cepheids

Cepheids play a key role in the knowledge of cosmological distances through the famous Period-Luminosity law. This relation has been calibrated from the nearest stars, but AMBER, which will be able to measure diameters for a larger sample, will provide a better calibration of the PL law following the application of the Baade-Wesselink technique. Indeed, some promising works, obtained with VINCI, have already refined the distances for a few Cepheids.[19]

However, in order to derive properly the basic elements, it is necessary to consider first the pulsation motions. For instance, the Hα absorption line often shows two components, sometimes superposed to an emission feature. A high resolution spectroscopic monitoring of this line for the long period Cepheid star ℓ Car[20] has shown the presence of emission which appears, depending on the pulsation phase, red- and/or blue-shifted. AMBER should bring new insights on the origin of such an emission, either due to a shock wave or circumstellar material. In addition, the propagation of shock waves in stellar atmospheres is yet poorly known. Here again, AMBER should constrain some parameters such as the location of the layers apart the shock front.

4.3. Mass Determination

Mass is THE fundamental stellar parameter, and AMBER (and later PRIMA) will provide orbits that will allow mass determination for many systems. The destabilizing mechanism in most pulsating stars is based on an opacity modulation in the transition zone, and strongly depends on the stellar internal structure. Masses are generally poorly known, and photometric calibrations are still very inaccurate.

Moreover, applying a linear adiabatic stability analysis leads to the destabilisation of many modes, whereas only a few ones are observed. Therefore, some selection mechanism must act, such as age, rotation, magnetism... But the important parameter is mass which affects the location of the driving zone in the enveloppe. For instance, concerning B stars, Balona et al.[21] already showed that for a given age, the frequency of excited modes is strongly correlated with mass. Therefore, AMBER will provide new constrains on models, which is very important in the context of asteroseimology, in particular for the COROT mission.

5. PROBING THE DISK OF BE AND B[E] STARS

Be stars are hot and fast rotating stars surrounding by an extended circumstellar envelope of hydrogen gas. In a given stellar field approximately 20 % of the B stars are in fact Be stars. This percentage can be much higher in some young clusters where up to 60-70 % of the B stars are showing the Be phenomenon, i.e. Balmer lines in emission and infrared excess. These stars are very bright and over luminous compared to B "normal" stars due to the presence of their circumstellar envelope. In young clusters with many Be stars, the luminosity function may seem to contain too massive stars, leading to an artificially top-heavy Initial Mass Function (IMF).

What causes B stars to become Be stars is not yet well understood. The proposed mechanisms include the wind compressed disc model of Bjorkman & Cassinelli,[22] the SIMECA code[23,24] based on the bi-stability effect,[25] non-radial pulsations, magnetic activity and binarity. The optical/infrared and the ultraviolet observations of Be stars have been widely interpreted as being the evidence for the existence of two quite distinct regions in the circumstellar envelopes of these objects: a dense rotating equatorial region and a diluted polar regions which expands with velocities[26] that may reach 1500 km/s. The equatorial region seem to present a very low radial expansion, as considered by Poeckert[27] and by Waters and co-workers.[28–30]

One of the challenging questions on Be stars is the geometry of their disk and particularly their opening angle, for which there is still an active debate. Most authors have considered geometrically thin disks (half opening angle of 2-5 degrees), and interferometric observation have given some upper limits around 20 degrees. However such narrow disks hypothesis face several problems, and the current set of observations do not provide a unique interpretation on the circumstellar geometry, even by performing a deep statistical investigation of the observations for a large sample of Be stars.[31] Interferometry in the visible has been used successfully to study the circumstellar environment of Be stars.[24,32–35] By observing Be stars at wavelengths as long as 20 μm, Gehrz[36] demonstrated that the Be MIR excess is due to free-free emission of the hydrogen envelop. The model from Waters[28] has then been successful to explain the near and far IR observations and is coherent also with polarization data. Thanks to the SIMECA code developed by Stee et al.[23,24,37] we are able to compute hydrogen line profiles, energy distribution, intensity maps and corresponding visibility curves for a large set of parameters which allows us to model both the NIR and the MIR emission from these stars.

B[e] are hot supergiants showing an important excess in the infrared due to the presence of hot circumstellar dust around. These stars exhibit also the so-called 'Be Phenomenon', but show forbidden also lines in their spectrum. Zickgraf et al.[38] proposed a model for the LMC B[e] supergiant R126 consisting of a fast wind in the polar regions and a dense and slow wind in the equatorial region where the dust is formed. Whilst there is a good physical explanation of the fast polar wind[39] the formation mechanism (and indeed the structure) of the dense equatorial flow is still largely unknown. An excellent attempt at explaining the equatorial flow has been made by Lamers & Pauldrach[40] (bi-stability model), which has been recently advanced by Pelupessy et al.[41] (2000) who suggest that wind compression due to its rotation[22] may also play a part in the generation of the disc. Observations of the peculiar star HD 62623 at the Keck telescope with the aperture masking interferometry[42] showed an envelope that seems partially resolved in the near infrared.[43] A next generation of Be model (SIMECA II) will be dedicated to the case of the B[e] stars. Based on the scheme of Zickgraf et al.,[38] this model assumes the central star as a classical Be star with two quite distinct regions in the circumstellar envelopes. The thermal infrared excess is produced in the outer parts of the equatorial region where the temperature allows the formation of dust grains. To produce dust, two criteria need to be fulfilled: the temperature of the gas must be lower than the sublimation temperature of the dust (around 1500 K depending on the chemical composition of the dust), and secondly, the number density of the species involved in the formation of the dust needs to be above a critical value. Porter (2002) showed recently that there is a significant problem with the dust emission in that the optical depths where dust forms is not large enough to generate the observed emission. It appears from his results that both the 'standard' equatorial wind model and the viscous disc model have trouble in generating the continuum emission for sgB[e] stars. The key parameter seems the density profile necessary to account for the dust generation, and this can be checked only with optical interferometry in the optical-near-IR range with AMBER and for the external and colder environment with MIDI. For both spectral types NIR/MIR interferometric observations should represent the strongest mean to constrain their internal/external environment.

REFERENCES

1. R. G. Petrov, F. Malbet, G. Weigelt, F. Lisi, P. Puget, P. Antonelli, U. Beckmann, S. Lagarde, E. Lecoarer, S. Robbe-Dubois, G. Duvert, S. Gennari, A. Chelli, M. Dugue, K. Rousselet-Perraut, M. Vannier, and D. Mourard, "Using the near infrared VLTI instrument AMBER," in *Interferometry for Optical Astronomy II. Edited by Wesley A. Traub . Proceedings of the SPIE, Volume 4838, pp. 924-933 (2003).*, pp. 924–933, Feb. 2003.
2. R. G. Petrov and The AMBER Consortium, "Introducing the near infrared VLTI instrument AMBER to its users," *Ap&SS* **286**, pp. 57–67, 2003.
3. F. Malbet, T. Bloecker, R. Foy, D. Fraix-Burnet, P. Mathias, A. Marconi, J. Monin, R. G. Petrov, P. Stee, L. Testi, and G. Weigelt, "Astrophysical potential of the AMBER/VLTI instrument," in *Interferometry for Optical Astronomy II. Edited by Wesley A. Traub . Proceedings of the SPIE, Volume 4838, pp. 917-923 (2003).*, pp. 917–923, Feb. 2003.
4. R. R. J. Antonucci and J. S. Miller, "Spectropolarimetry and the nature of NGC 1068," *ApJ* **297**, pp. 621–632, Oct. 1985.
5. J. H. Krolik and M. C. Begelman, "Molecular tori in Seyfert galaxies - Feeding the monster and hiding it," *ApJ* **329**, pp. 702–711, June 1988.
6. G. L. Granato, L. Danese, and A. Franceschini, "Thick Tori around Active Galactic Nuclei: The Case for Extended Tori and Consequences for Their X-Ray and Infrared Emission," *ApJ* **486**, pp. 147–+, Sept. 1997.
7. M. Nenkova, Ž. Ivezić, and M. Elitzur, "Dust Emission from Active Galactic Nuclei," *ApJl* **570**, pp. L9–L12, May 2002.
8. M. Wittkowski, Y. Balega, T. Beckert, W. J. Duschl, K.-H. Hofmann, and G. Weigelt, "Diffraction-limited 76mas speckle masking observations of the core of NGC 1068 with the SAO 6m telescope," *A&A* **329**, pp. L45–L48, Jan. 1998.
9. A. J. Weinberger, G. Neugebauer, and K. Matthews, "Diffraction-limited Imaging and Photometry of NGC 1068," *AJ* **117**, pp. 2748–2756, June 1999.
10. G. Weigelt et al., "Diffraction-Limited Bispectrum Speckle Interferometry of the Nuclear Region of the Seyfert Galaxy NGC 1068 in the H and K' Bands'," *A&A* **in press**, 2004.
11. M. Wittkowski, P. Kervella, R. Arsenault, F. Paresce, T. Beckert, and G. Weigelt, "VLTI/VINCI observations of the nucleus of NGC 1068 using the adaptive optics system MACAO," *A&A* **418**, pp. L39–L42, Apr. 2004.
12. D. Rouan, F. Rigaut, D. Alloin, R. Doyon, O. Lai, D. Crampton, E. Gendron, and R. Arsenault, "Near-IR images of the torus and micro-spiral structure in NGC 1068 using adaptive optics," *A&A* **339**, pp. 687–692, Nov. 1998.
13. D. Rouan, F. Lacombe, E. Gendron, D. Gratadour, Y. Clénet, A.-M. Lagrange, D. Mouillet, C. Boisson, G. Rousset, T. Fusco, L. Mugnier, M. Séchaud, N. Thatte, R. Genzel, P. Gigan, R. Arsenault, and P. Kern, "Hot Very Small dust Grains in ¡ASTROBJ¿NGC 1068¡/ASTROBJ¿ seen in jet induced structures thanks to VLT/NACO adaptive optics," *A&A* **417**, pp. L1–L4, Apr. 2004.
14. J. F. Gallimore, S. A. Baum, and C. P. O'Dea, "A direct image of the obscuring disk surrounding an active galactic nucleus.," *Nature* **388**, pp. 852–854, 1997.
15. W. Jaffe, K. Meisenheimer, H. J. A. Röttgering, C. Leinert, A. Richichi, O. Chesneau, D. Fraix-Burnet, A. Glazenborg-Kluttig, G.-L. Granato, U. Graser, B. Heijligers, R. Köhler, F. Malbet, G. K. Miley, F. Paresce, J.-W. Pel, G. Perrin, F. Przygodda, M. Schoeller, H. Sol, L. B. F. M. Waters, G. Weigelt, J. Woillez, and P. T. de Zeeuw, "The central dusty torus in the active nucleus of NGC 1068," *Nature* **429**, pp. 47–49, May 2004.
16. R. D. Blandford, H. Netzer, L. Woltjer, T. J.-L. Courvoisier, and M. Mayor, *Active Galactic Nuclei*, Saas-Fee Advanced Course 20. Lecture Notes 1990. Swiss Society for Astrophysics and Astronomy, XII, 280 pp. 97 figs.. Springer-Verlag Berlin Heidelberg New York, 1990.
17. B. M. Peterson, "Overview of Reverberation Mapping: Progress and Problems," in *ASP Conf. Ser. 69: Reverberation Mapping of the Broad-Line Region in Active Galactic Nuclei*, pp. 1–+, 1994.

18. S. Kaspi, P. S. Smith, H. Netzer, D. Maoz, B. T. Jannuzi, and U. Giveon, "Reverberation Measurements for 17 Quasars and the Size-Mass-Luminosity Relations in Active Galactic Nuclei," *ApJ* **533**, pp. 631–649, Apr. 2000.
19. P. Kervella, N. Nardetto, D. Bersier, D. Mourard, and V. Coudé du Foresto, "Cepheid distances from infrared long-baseline interferometry. I. VINCI/VLTI observations of seven Galactic Cepheids," *A&A* **416**, pp. 941–953, Mar. 2004.
20. I. K. Baldry, M. M. Taylor, T. R. Bedding, and A. J. Booth, "H alpha profile variations in the long-period Cepheid L Carinae," *MNRAS* **289**, pp. 979–985, Aug. 1997.
21. L. A. Balona, W. A. Dziembowski, and A. Pamyatnykh, "The structure of the instability strip and mode identification for beta CEP stars in three young open clusters," *MNRAS* **289**, pp. 25–36, July 1997.
22. J. E. Bjorkman and J. P. Cassinelli, "Equatorial disk formation around rotating stars due to Ram pressure confinement by the stellar wind," *ApJ* **409**, pp. 429–449, May 1993.
23. P. Stee and F. X. de Araujo, "Line profiles and intensity maps from an axi-symmetric radiative wind model for Be stars," *A&A* **292**, pp. 221–238, Dec. 1994.
24. P. Stee, F. X. de Araujo, F. Vakili, D. Mourard, L. Arnold, D. Bonneau, F. Morand, and I. Tallon-Bosc, "γ Cassiopeiae revisited by spectrally resolved interferometry.," *A&A* **300**, pp. 219–+, Aug. 1995.
25. H. J. G. L. M. Lamers, T. P. Snow, and D. M. Lindholm, "Terminal Velocities and the Bistability of Stellar Winds," *ApJ* **455**, pp. 269–+, Dec. 1995.
26. J. M. Marlborough, "Rotationally-enhanced stellar winds," in *IAU Colloq. 92: Physics of Be Stars*, pp. 316–335, 1987.
27. R. Poeckert and J. M. Marlborough, "A model for Gamma Cassiopeiae," *ApJ* **220**, pp. 940–961, Mar. 1978.
28. L. B. F. M. Waters, "The density structure of discs around Be stars derived from IRAS observations," *A&A* **162**, pp. 121–139, July 1986.
29. L. B. F. M. Waters, J. Cote, and H. J. G. L. M. Lamers, "IRAS observations of Be stars. II - Far-IR characteristics and mass loss rates," *A&A* **185**, pp. 206–224, Oct. 1987.
30. L. B. F. M. Waters and J. M. Marlborough, "Constraints on Be star wind geometry by linear polarisation and IR excess," *A&A* **256**, pp. 195–204, Mar. 1992.
31. B. Yudin, Y. Balega, T. Blöcker, K.-H. Hofmann, D. Schertl, and G. Weigelt, "Speckle interferometry and radiative transfer modelling of the Wolf-Rayet star ¡ASTROBJ¿WR 118¡/ASTROBJ¿," *A&A* **379**, pp. 229–234, Nov. 2001.
32. C. Thom, P. Granes, and F. Vakili, "Optical interferometric measurements of Gamma Cassiopeiae's envelope in the H-alpha line," *A&A* **165**, pp. L13–L15, Sept. 1986.
33. A. Quirrenbach, D. F. Buscher, D. Mozurkewich, C. A. Hummel, and J. T. Armstrong, "Maximum-entropy maps of the Be shell star zeta Tauri from optical long-baseline interferometry," *A&A* **283**, pp. L13–L16, Mar. 1994.
34. A. Quirrenbach, C. A. Hummel, D. F. Buscher, J. T. Armstrong, D. Mozurkewich, and N. M. Elias, "The Asymmetric Envelope of gamma Cassiopeiae Observed with the MK III Optical Interferometer," *ApJl* **416**, pp. L25+, Oct. 1993.
35. A. Quirrenbach, K. S. Bjorkman, J. E. Bjorkman, C. A. Hummel, D. F. Buscher, J. T. Armstrong, D. Mozurkewich, N. M. Elias, and B. L. Babler, "Constraints on the Geometry of Circumstellar Envelopes: Optical Interferometric and Spectropolarimetric Observations of Seven Be Stars," *ApJ* **479**, pp. 477–+, Apr. 1997.
36. R. D. Gehrz, J. A. Hackwell, and T. W. Jones, "Infrared observations of Be stars from 2,3 to 19,5 microns.," *ApJ* **191**, pp. 675–684, Aug. 1974.
37. P. Stee, F. Vakili, D. Bonneau, and D. Mourard, "On the inner envelope of the Be star gamma Cassiopeiae," *A&A* **332**, pp. 268–272, Apr. 1998.
38. F.-J. Zickgraf, B. Wolf, O. Stahl, C. Leitherer, and G. Klare, "The hybrid spectrum of the LMC hypergiant R126," *A&A* **143**, pp. 421–430, Feb. 1985.
39. J. I. Castor, D. C. Abbott, and R. I. Klein, "Radiation-driven winds in Of stars," *ApJ* **195**, pp. 157–174, Jan. 1975.

40. H. J. G. Lamers and A. W. A. Pauldrach, "The formation of outflowing disks around early-type stars by bi-stable radiation-driven winds," *A&A* **244**, pp. L5–L8, Apr. 1991.
41. I. Pelupessy, H. J. G. L. M. Lamers, and J. S. Vink, "The radiation driven winds of rotating B[e] supergiants," *A&A* **359**, pp. 695–706, July 2000.
42. P. G. Tuthill, J. D. Monnier, W. C. Danchi, E. H. Wishnow, and C. A. Haniff, "Michelson Interferometry with the Keck I Telescope," *PASP* **112**, pp. 555–565, Apr. 2000.
43. J. Bittar, P. Tuthill, J. D. Monnier, B. Lopez, W. Danchi, and P. Stee, "High angular resolution observations in the near infrared and modeling of the peculiar envelope of HD 62623," *A&A* **368**, pp. 197–204, Mar. 2001.